

Photocatalytic Hydrogels with a High Transmission Polymer Network for Pollutant Remediation

Thomas Kuckhoff, Katharina Landfester, Kai A. I. Zhang,* and Calum T. J. Ferguson*



Cite This: *Chem. Mater.* 2021, 33, 9131–9138



Read Online

ACCESS |



Metrics & More

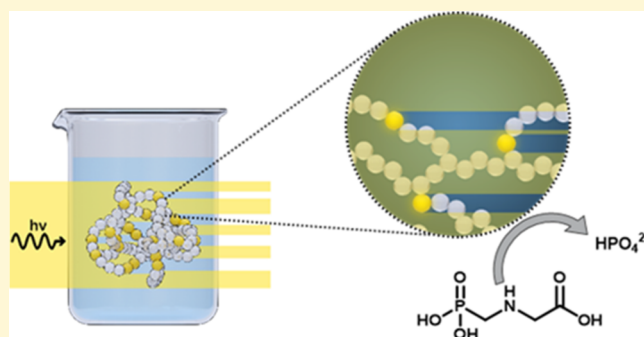


Article Recommendations



Supporting Information

ABSTRACT: Efficient heterogeneous and metal-free photocatalysts have recently been targeted as reusable materials for pollutant remediation. However, poor light penetration into photocatalytic materials currently limits modern photocatalytic systems due to uneven performance across the photocatalytic material and inefficient light usage. Here, we present a classical photocatalytic polymer hydrogel composed of a high transmittance polymer network and small conjugated photocatalytic moieties. Radical copolymerization of a photocatalytically active benzothiazole acrylamide monomer with water-compatible *N,N*-dimethylacrylamide produced a photocatalytic hydrogel where only the photocatalytic moiety absorbs visible light. The photocatalytic hydrogel network enables easy partitioning of pollutants into the gel network, where they are photocatalytically degraded. The versatility and reusability of the photocatalytic material were demonstrated for degradation of both inorganic metal and organic contaminants, including *N*-(phosphonomethyl)glycine (glyphosate), the most commonly used herbicide. Furthermore, the potential of this material was explored in large-scale experiments, where glyphosate could be readily photodegraded at a half liter scale.



INTRODUCTION

Sunlight is an abundant and renewable energy source that can be utilized to facilitate a broad range of chemical reactions. Inspiration can be taken from nature, where sunlight is used as a clean energy source in photosynthesis. To mimic this natural process, numerous heterogeneous photocatalytic materials have been produced and implemented into a wide range of chemical applications, including water splitting,^{1–7} photoredox reactions,^{8–13} CO₂ reduction,^{14–17} photodynamic therapy,^{18–21} and wastewater purification.^{22–26}

Wastewater treatment is an important part of a sustainable water management and integral for an ever-increasing global population. The recycling of water by purification through separation or degradation of pollutants is therefore essential. Unfortunately, conventional sewage treatment systems are not able to efficiently remove new emerging molecular pollutants.^{27,28} Photocatalysis has therefore received increasing attention for water contaminant degradation.^{23–26} Photocatalysis enables ecologically friendly wastewater purification, by photodegradation, facilitated by the generation of highly oxidizing species. Previously, heterogeneous photocatalysts have been used for wastewater treatment based on different materials ranging from inorganic materials such as TiO₂ to nanodots and conjugated polymers.^{29–33}

Nevertheless, one of the most prominent drawbacks of heterogeneous photocatalytic materials is the low photon penetration depth into the photocatalytic material. A low and uneven irradiation is often observed in bulk applications,

lowering overall irradiation efficiency and, therefore, photodegradation.^{34–37} This may be due to light incident on the heterogeneous material being scattered. Furthermore, light penetration into heterogeneous photocatalytic materials is often limited, leading to inefficient usage of the photocatalytic material, especially in large-scale applications. This poor penetration may be due to the absorption of light by nonphotocatalytically active materials.

Ideally, a heterogeneous photocatalytic system for water purification would be created that could be easily recovered and reused. Furthermore, visible light incident on the material should be homogeneously absorbed across the photocatalytic material and not be obstructed by the supporting structure. Additionally, the photocatalytic material must be compatible with aqueous environments, allowing for easy partitioning of reagents into and out of the photocatalytic material. Therefore, the synthesis of a high transmittance, hydrophilic, porous substrate in combination with a homogeneously distributed photocatalytic moiety may yield more efficient photocatalysts.^{38–42}

Received: June 24, 2021

Revised: November 4, 2021

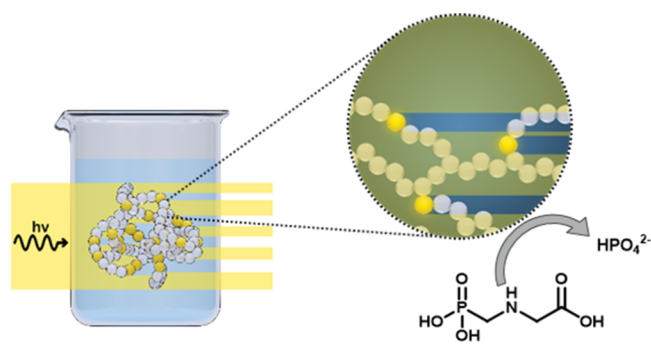
Published: November 21, 2021



Hydrogels are hydrophilic networks, which contain over 90% water, and have a high biocompatibility and allow for easy substrate diffusion into the material. As a result, hydrogels have been widely studied for biomedical applications, including drug delivery.^{43–45} Moreover, transparent hydrogels have been used in soft contact lenses.^{44,46,47} Compared to rigid porous polymers, hydrogels can often be more readily swollen in water. This swollen network allows for easy diffusion of molecules into the gel network. As a result, hydrogels have been studied for use in wastewater remediation, as their properties allow for the absorbance of dyes and organic pollutants.^{48,49} Hydrogels can easily be synthesized through radical polymerization without need for exceedingly toxic materials or heavy metals. Therefore, transparent hydrogels would be a desirable polymer matrix for the incorporation of the photocatalyst. Recently, our group has described the synthesis of a new class of photocatalytic classical polymers.^{50–52} The copolymerization of photocatalytic small molecules, modified with vinyl functionality, and classical monomers, combines the versatility of classical polymers with photocatalytic activity. This combination produces a new hybrid material class of photocatalytically active polymers.⁵³

Here, we have designed photocatalytic hydrogels, where only the photocatalytic moieties absorb visible light, as illustrated in Scheme 1. The copolymerization of photo-

Scheme 1. High Transmittance Photocatalytic Hydrogels Allow for Easy Light Penetration into the Photocatalytic System for Efficient Water Remediation; Light Is Not Reflected or Absorbed by the Polymer Network and Is, Therefore, Available for Photocatalytic Reactions



catalytic small molecules with classical monomers produces highly efficient photocatalytic gels. A *N,N*-dimethylacrylamide (DMAA)-based gel was selected due to the high transmittance of visible light through the gel, allowing more energy to be available for the photocatalytic units. A donor–acceptor type photocatalytic unit containing benzothiadiazole (~2 mol %) was copolymerized into the gel material, with leaching of the photocatalytic unit inhibited. Due to its intrinsic properties, the hydrogel allows for a high substrate diffusion into the substrate, while the high transmittance of the polymer network does not interfere with the absorbance properties of the photocatalytic units. The photocatalytic hydrogel was used for the photodegradation of model wastewater pollutants. To showcase the broad application range and versatility, the photocatalytic hydrogel was investigated for the photo-oxidation of *N*-(phosphonomethyl)glycine (glyphosate), rhodamine B, and organic sulfurs as well as the photoreduction of inorganic pollutants, namely, heavy metal contaminants in the form of chromium (VI). Furthermore, the scalability of the material

was investigated for gram-scale photodegradation of glyphosate.

EXPERIMENTAL SECTION

Materials. 4,7-Dibromobenzo[*c*][1,2,5]thiadiazole was purchased from Combi-Blocks. Phenylboronic acid was purchased from TCI Germany. Tetrakis(triphenylphosphine)palladium(0), 4-aminophenylboronic acid pinacol ester, acryloyl chloride, rhodamine B, dimethylacrylamide, *N,N'*-methylenebisacrylamide, DMSO-*d*₆, deuterium oxide, and 4-methoxyphenyl methylsulfide were purchased from Sigma-Aldrich. DCM-*d*₂ was purchased from Deutero. Methyl phenyl sulfide, 4-methylphenyl methyl sulfide, and 4-chlorophenyl methyl sulfide were purchased from Alfa Aesar. *N*-(Phosphonomethyl)glycine was purchased from Molekula and chromium trioxide from Acros Organics. All the chemicals and solvents were used without purification.

Characterization. ¹H, ¹³C, and ³¹P NMR spectra were measured using a Bruker Avance 300 MHz. The solid-State ¹³C CP MAS NMR measurement was carried out using a Bruker Avance II solid-state NMR spectrometer operating at 300 MHz. FT-IR measurements were conducted with a Bruker Tensor II FTIR spectrometer. Gas chromatography was performed on a Shimadzu GC-2010 plus gas chromatograph and analyzed with a QP2010 ultra mass spectrometer. Fluorescence microscopy was performed on a Leica DMi8 inverted light microscope. UV/Vis-absorption spectra were measured on a Cary 60 UV–Vis/NIR spectrometer. For cyclic voltammetry measurements, a Metrohm Autolab PGSTAT204 potentiostat/galvanostat, with a glassy carbon electrode as the working electrode, Hg/HgCl₂ electrode as the reference electrode, and a platinum wire as the counter electrode, was used. DFT calculations were carried out using the Gaussian 09 (rB3LYP, basis set: 6-31G).

Synthesis of PDMAA-BTPH₂. DMAA (0.2 g, 2.0 mmol), *N,N'*-methylenebisacrylamide (6.2 mg, 40.3 μmol), and *N*-(4-(7-phenylbenzo[*c*][1,2,5]thiadiazol-4-yl)phenyl)acrylamide (14.4 mg, 40 μmol) were dissolved in 1 mL of DMF. AIBN (3.31 mg, 20 μmol) was added, and the solution was degassed using argon. The solution was heated at 80 °C overnight. The resulting polymer was excessively washed with THF and purified via dialysis against water/LiCl and pure water.

Synthesis of Linear-PDMAA-BTPH₂. DMAA (0.2 g, 2.0 mmol) and *N*-(4-(7-phenylbenzo[*c*][1,2,5]thiadiazol-4-yl)phenyl)acrylamide (14.4 mg, 40 μmol) were dissolved in 1.5 mL of DMF. AIBN (3.31 mg, 20 μmol) was added, and the solution was degassed using argon. The solution was heated at 80 °C overnight. The resulting polymer was precipitated in diethyl ether. *M_n* (14,403 g/mol) *D* 2.8.

Rhodamine B Degradation. To a rhodamine B solution (100 mg/L) in 4 mL of water, the hydrogel (29 mg, photocatalyst 1.9 mol %, 5.2 μmol) was added. The vial was irradiated with blue LED light (power: 0.16 W cm⁻², λ 460 nm) under stirring. UV/Vis samples were taken periodically to track the degradation rates of the dye.

Photoreduction of Chromium Trioxide. To a Cr^{VI}+O₃ solution (25 mg/L, 0.125 mg, 1.25 μmol) in 5 mL of water, the hydrogel (15 mg, photocatalyst 1.9 mol %, 2.7 μmol) was added. The solution was degassed by nitrogen bubbling and irradiated with a blue LED light (power: 0.16 W cm⁻², λ 460 nm). The Cr^{VI} concentration was determined via UV/Vis absorbance using a diphenylcarbazide solution in acetone (0.25 wt %). Therefore, 0.5 mL of the Cr^{VI}+O₃ solution was centrifuged and added to 5 mL of 0.2 M H₂SO₄. Diphenylcarbazide (0.1 mL) was added, stirred for 2 min, and monitored through UV/Vis spectroscopy.

Photoreduction of Chromium Trioxide Recycle Experiment. To a Cr^{VI}+O₃ solution (25 mg/L, 0.125 mg; 1.25 μmol) in 5 mL of water, the hydrogel (15 mg photocatalyst 1.9 mol %, 2.7 μmol) was added. The solution was degassed by nitrogen bubbling and irradiated with a blue LED light (power: 0.16 W cm⁻², λ 460 nm) for 2 h. The Cr^{VI} concentration was determined after 2 h as mentioned above. New Cr^{VI}+O₃ solution was added, and the experiment was repeated for five cycles.

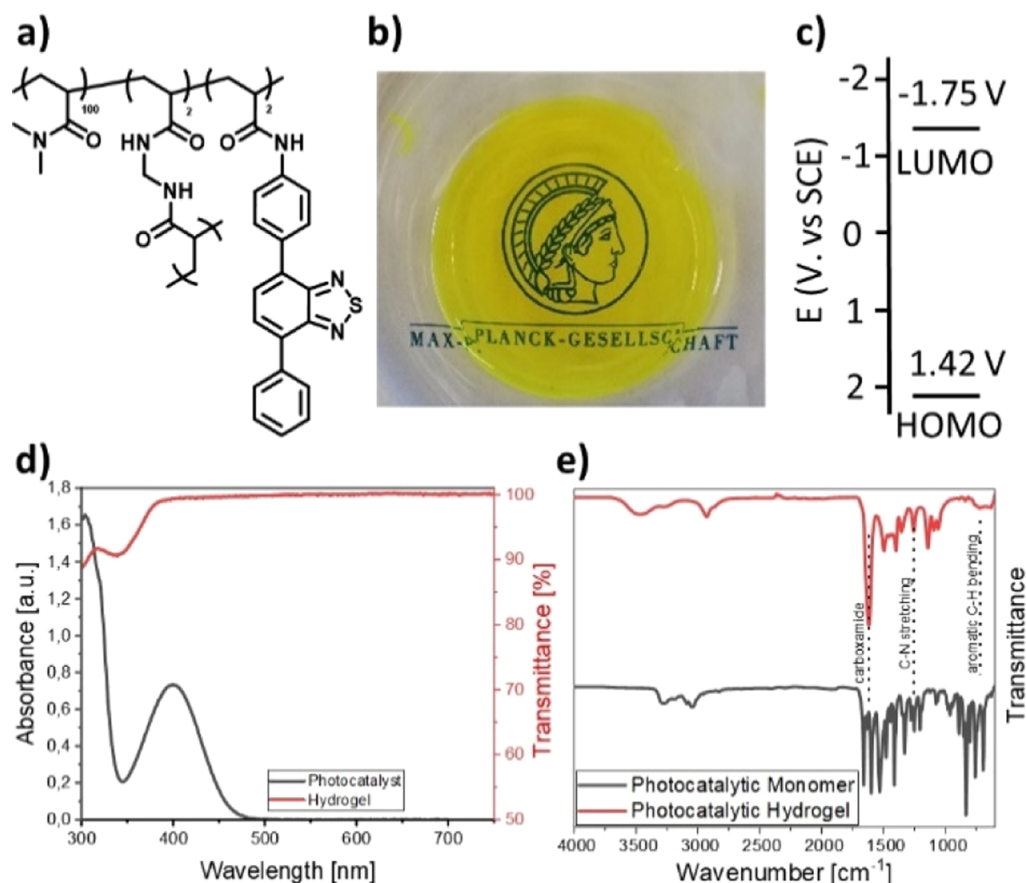


Figure 1. High transmittance hydrogel (a) molecular structure of the designed hydrogel, (b) synthesized high transmittance photocatalytic hydrogel, (c) calculated HOMO/LUMO Level, (d) (red) transmittance spectra of the hydrogel without the photocatalyst and (black) absorbance spectra of the photocatalyst. (e) FTIR of the photocatalytic hydrogel and the synthesized photocatalytic monomer.

Photodegradation *N*-(phosphonomethyl)glycine. To D_2O (5 mL), *N*-(phosphonomethyl)glycine (12.5 mg; $74 \mu\text{mol}$), NaOH (400 μL , 2 M), and the hydrogel (25 mg, 1.9 mol % photocatalyst 4.5 μmol) or linear-PDMAA-BTPH2 (25 mg) were added. The mixture was bubbled with O_2 under stirring for 5 min. The vial was then irradiated with blue LED light (power: 0.16 W cm^{-2} , λ 460 nm) under an oxygen atmosphere. The sample was centrifuged and analyzed via ^{31}P NMR.

Large-Scale Photodegradation of *N*-(Phosphonomethyl)glycine. To H_2O (500 mL), *N*-(phosphonomethyl)glycine (1 g; 5.9 mmol), NaOH (40 mL, 2 M) and the hydrogel (2.5 g, 1.9 mol % photocatalyst 450 μmol) were added. The mixture was bubbled with O_2 under stirring for 30 min. The flask was then irradiated with blue LED lights (power: 0.16 W cm^{-2} , λ 460 nm) under an oxygen atmosphere. Samples were taken every 5 h and freeze-dried. The residue was taken up in 1 mL of D_2O , centrifuged, and analyzed via ^{31}P NMR.

Photo-oxidation of Methyl Phenyl Sulfide or Its Derivatives. Methyl phenyl sulfide or its derivatives (30 mM) and the photocatalytic hydrogel (10 mg, photocatalyst 1.9 mol %, 1.8 μmol photocatalyst) were dispersed in 10 mL of water. The mixture was bubbled with O_2 under stirring. The vial was irradiated with blue LED light (power: 0.16 W cm^{-2} , λ 460 nm) for 22 h. The sample was extracted with DCM and dried over MgSO_4 . Products and conversion were determined by GC-MS and purified via column chromatography (PE/EtAc = 1:1).

Scavenger Test. Methyl phenyl sulfide (30 mM), scavenger (45 mM), and photocatalytic hydrogel (10 mg, photocatalyst 1.9 mol %, 1.8 μmol photocatalyst) were dispersed in 10 mL of water. The mixture was bubbled with O_2 under stirring. The vial was irradiated with blue LED light (power: 0.16 W cm^{-2} , λ 460 nm) for 22 h. The

sample was extracted with DCM and dried over MgSO_4 . Products and conversion were determined by GC-MS.

RESULTS AND DISCUSSION

Photocatalytic hydrogels were synthesized using radical polymerization, allowing for a quick and cost-efficient synthesis. The hydrogel matrix was constructed from DMAA and cross-linked using *N,N'*-methylenebisacrylamide (Figures 1a and S1). This gel network was selected due to its high transmittance of visible light, preventing energy loss due to light scattering and absorption of nonphotocatalytically active portions of the hydrogel (Figure 1b). The absorbance of the polymer matrix was analyzed via transmittance measurement displaying a high transmittance of 95–99% between 400 and 800 nm, while in the UV region below 400 nm, the hydrogel absorbance increases (Figure 1c).

The *N*-(4-(7-Phenylbenzo[*c*][1,2,5]thiadiazol-4-yl)phenyl)-acrylamide photocatalytic monomer was copolymerized into the hydrogel network (Figures S2 and S3), leading to a high transmittance photocatalytic hydrogel. The photocatalytic monomer displayed a peak absorption at 400 nm with the absorption extended to 470 nm (Figure 1c). The photocatalytic monomer was designed and synthesized to include acrylamide functionality to ensure that the propagation rate of polymerization for each monomer was in the same order of magnitude, which is integral to produce a homogenous photocatalytic hydrogel. Density functional theory (DFT) calculations of the photocatalytic monomer were used to

predict the energy and electron density of the highest occupied molecule orbital (HOMO) and lowest unoccupied molecule orbital (LUMO) (Figures 1c and S4). The HOMO and LUMO levels were 1.42 and -1.75 V versus SCE, respectively. From cyclic voltammetry, the LUMO level of the photocatalytic hydrogel was determined to be -1.30 versus SCE, similar to the calculated value (Figure S5). The difference in measured and calculated LUMO levels is believed to be due to the calculated value being for the monomer, not for the polymerized form. Previously published DTF calculation and CV measurements of vinyl functionalized benzothiadiazol monomers display comparable HOMO/LUMO energies, indicating stable energy levels regardless of the chosen functionalization.⁵¹ This enables different functionalities to be incorporated and copolymerization with various monomers with differing propagation rates to be achieved.

To verify the inclusion of the photocatalytic monomer within the polymer, solid-state NMR (ssNMR) and Fourier transform infrared (FTIR) spectroscopy were carried out. ¹³C-ssNMR spectroscopy shows a peak at 37 ppm corresponding to the polymer backbone and the methylamine groups. A strong peak was observed at 175 ppm due to the carbonyl group of each monomer. Aromatic peaks are observed between 125 and 160 ppm, which correspond to the photocatalytic monomer, showing that the active unit is indeed within the polymer hydrogel (Figure S6). FTIR analysis of the photocatalytic hydrogel and the photocatalytic monomer was undertaken (Figures 1e and S7). FTIR shows peaks at 2930 cm^{-1} for the $-\text{CH}_2$ and $-\text{CH}_3$ stretch vibration. The peak at 1620 cm^{-1} can be assigned to the stretching of the carboxamide. Signals at around 1500 cm^{-1} are attributed to the $-\text{CH}_3$ deformation, while the band at around 1260 cm^{-1} is due to C-N stretching. Due to the low concentration of photocatalytic moiety within the hydrogel (1.9 mol %), the peaks corresponding to the conjugated photocatalytic monomer are not easily discerned.

UV/Vis absorbance spectra of the dried hydrogel showed peak absorption at 420 nm extending to 510 nm, indicating a red shift compared to the pure photocatalytic monomer in DMSO (Figure S9). To further analyze the photocatalytic behavior of the synthesized hydrogel, photocurrent measurements were conducted (Figure S10). In five repeating cycles, a photoinduced conductivity was measured, presenting a clear photoresponsive behavior.

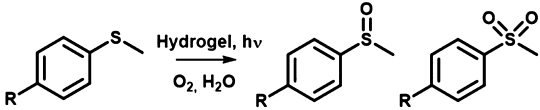
The dried photocatalytic hydrogel readily swells in water. The degree of swelling was determined by fluorescence spectroscopy. Here, the photocatalytic units incorporated into the gel network enable easy monitoring of the swelling process. The photocatalytic hydrogel swelled in water by a factor of 2.5 within 30 s (Figure S11), and as expected, we see an even distribution of the photocatalyst across the gel network. Furthermore, no leaching of the photocatalytic moiety was observed during the swelling process. The degree of swelling of the hydrogel was obtained over three swelling cycles, where the weight gain was measured and the water content was determined, showing that the fully swollen gel reaches a water content of 92% (Figures S12 and 13).

Water pollutants can be classified into two categories, organic and inorganic. Here, we have determined the potential of the high transmittance photocatalytic hydrogel for remediation of both pollutant classes. Initially, we investigated the degradation of organic pollutants, including small molecule pollutants and industrially relevant agrochemical-based water

pollutants. The photocatalytic degradation of an organic dye molecule, rhodamine B, was undertaken. Here, over 95% of the aqueous organic dye was removed within 4 h (Figures S14 and S15) in the presence of the photocatalytic hydrogel. Following the successful degradation of simple dye molecules, the remediation of organosulfur containing compounds was targeted.

Organic sulfur-containing compounds are emerging pollutants in wastewater due to their increased presence in drug molecules.^{24,28,29} As a model methyl phenyl sulfide and its derivative were oxidized, as seen in Table 1. Over 99%

Table 1. Photocatalytic Oxidation of Methyl Phenyl Sulfide Through the Photocatalytic Hydrogel under Various Conditions^a



number	condition	conversion
1	R = -H	<99% (98:2)
2	no light	0%
3	no photocat	0%
4	no oxygen	2% (100:0)
5	R = -Me	<99% (94:6)
6	R = -OMe	<99% (95:5)
7	R = -Cl	<99% (93:6)

^aSulfide (30 mM), hydrogel (10 mg, 1.8 μmol photocatalyst), 10 mL H_2O , conversion determined by GC-MS.

conversion was obtained for the oxidation of methyl phenyl sulfide, with a selectivity of 98:2 toward the mono-oxidized sulfoxide. Furthermore, functional group tolerance was observed in reactions with substituted methyl phenyl sulfide molecules with only small changes in the selectivity (Table 1 and Figures S16–S23). All reactions could be conducted with low concentrations of the photocatalyst (sulfide 30 mM, hydrogel 10 mg, 1.9 mol % photocatalyst, 1.8 μmol) and with high conversions. Here, sulfide oxidation was found to be comparable to previously reported photocatalytic classical polymers in the absence of oxidants.⁵² Furthermore, the hydrogel described here performed similarly to metal-based $\text{Bi}_4\text{O}_3\text{Br}_2$ photocatalysts under blue light irradiation. Conversely, to the hydrogel-based systems TiO_2 based photocatalysts could be used for this reaction upon visible light irradiation.⁵⁴ Scavenger tests were performed to show that the oxidation observed is indeed photocatalytically driven. As expected, in the absence of light, oxygen, or photocatalyst, no conversion was detected (Table 1). Benzoquinone, sodium azide, potassium iodide, isopropanol, and copper chloride were used as a superoxide, singlet oxygen, vacant hole, hydroxyl radical, and electron scavengers, respectively. Here, scavengers for superoxide, singlet oxygen, and the vacant hole species had the highest impact on conversion. In the presence of benzoquinone, a superoxide ($\text{O}_2^{\cdot-}$) scavenger, the conversion to sulfoxide was reduced by 75%, whereas the addition of sodium azide did not decrease the conversion but led to a higher yield of the sulfone species (Figure S24).

Further to organic pollutants, inorganic pollutant remediation was also investigated. Next to organic compounds, heavy metals are one of the most common pollutants in industrial wastewater.^{55–57} Cr^{VI} is a nonbiodegradable pollutant and can

cause significant environmental damage due to its high toxicity and cancerous properties.^{58,59} We have utilized the high transmittance photocatalytic hydrogels to photoreduce Cr^{VI} to Cr^{III} under aqueous conditions. Water-soluble Cr^{VI} was successfully reduced to the less toxic and water-insoluble Cr^{III} , allowing for an easy precipitation of the pollutant and decontamination of the wastewater. The Cr^{VI} photoreduction was measured by complexation of Cr^{VI} with diphenylcarbazide and monitored using UV/Vis spectroscopy (Figure S25). Cr^{VI} was reduced to Cr^{III} in around 60 min under blue light irradiation with a conversion of over 92% (Figure 2a), while

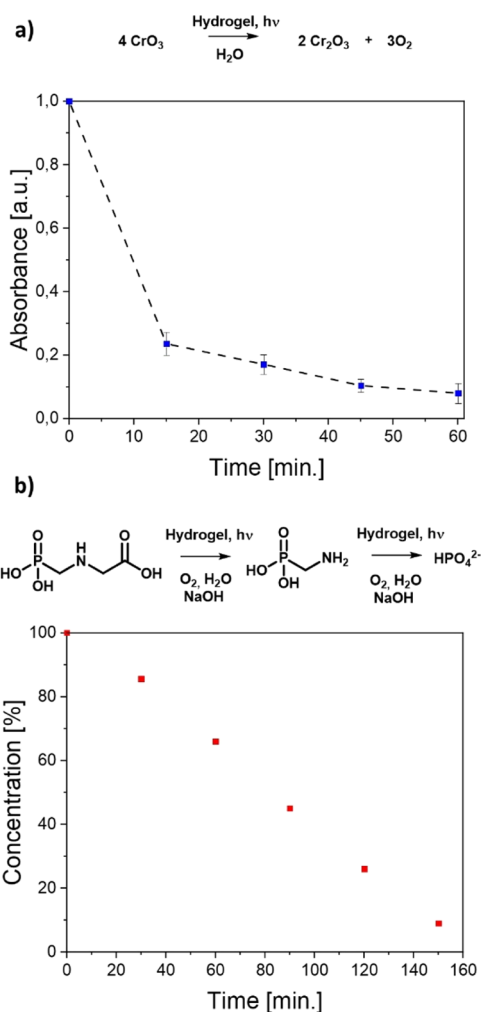


Figure 2. Photodegradation of glyphosate and chromium by the photocatalytic hydrogel: (a) chromium photoreduction over time under a N_2 atmosphere measured at 542 nm by complexation with diphenylcarbazide and (b) glyphosate degradation over time monitored via ^{31}P NMR.

control reactions in the dark and without the photocatalyst resulted in no conversion (Figures S26 and S27). Compared to published water-compatible fully conjugated microporous polyazulene photocatalysts, the photocatalytic hydrogel was found to have a higher efficiency requiring lower amounts of the photocatalytic active material.^{60,61}

The reusability of the photocatalytic hydrogel was demonstrated by conducting a recycling test for five repeating cycles. Cr^{VI} was again photoreduced in each run without a significant loss in efficiency, displaying that the material is

suitable for the efficient and stable heterogeneous photocatalyst (Figures S28 and S29).

To further demonstrate the versatility of the high transmittance photocatalytic hydrogel for remediation of pollutants in water, the photocatalytic degradation of glyphosate was investigated. Glyphosate is a nonselective organophosphate herbicide and the most widely used herbicide globally.^{62,63} Its over usage in agriculture has led to increasing concerns regarding dangerous levels of runoff into water systems such as rivers, lakes, and groundwater.^{64,65} Glyphosate has been found in surface and subsurface water sources and is known to be toxic to aquatic organisms.^{66–69} Therefore, it is important to produce methods that can readily degrade glyphosate in contaminated water.

Glyphosate is stable over a wide range of possible conditions and is not readily hydrolyzed in water.⁷⁰ We have demonstrated that high concentrations of glyphosate (2.5 mg/mL) can successfully be photodegraded, using low amounts of the photocatalytic hydrogel (5 mg/mL, 1.9 mol % photocatalyst, 0.9 μmol) under visible light. Over 90% degradation was observed after 2.5 h under basic conditions, while no significant degradation was observed under acid or neutral conditions. The reaction progression was analyzed via ^{31}P NMR with a glyphosate shift of 16.9 ppm, and the main degradation product, phosphate, emerges at 2.5 ppm. NMR analysis further indicates the existence of an intermediate at 19.3 ppm, which is likely to be (aminomethyl)phosphonic acid.⁷² To investigate the time-dependent degradation, kinetic measurement of the photodegradation of glyphosate was conducted via ^{31}P NMR spectroscopy, where a near-linear degradation of glyphosate was observed (Figures 2b and S30). Previously, degradation has been achieved using TiO_2 nanoparticles in a photoreactor. Here, a much larger concentration of TiO_2 nanoparticles (6 g/L) was required to achieve similar results as the hydrogel presented in this study.³⁰ Furthermore, previous pure organic systems have been shown to be insufficient for photocatalytic degradation of glyphosate, where $\text{BiO}_4/\text{PDA}/\text{g-C}_3\text{N}_4$ hybrid systems were required.⁷¹

Large-scale photocatalytic batch reactions are generally hindered by low light penetration depth and light scattering upon the heterogeneous photocatalyst leading to low overall efficiency. The high transmittance values of the synthesized hydrogel substrate should mitigate these issues, therefore, enabling large-scale photocatalysis. To showcase this, large-scale photodegradation of glyphosate was conducted (Figures 3 and S31) in a half liter batch reaction, and 1 g of glyphosate was photodegraded using the photocatalytic hydrogel leading to 60% conversion in the first 25 h and 78% after 45 h. Here, we observed an initial high rate of photodegradation that slowed overtime as the concentration of glyphosate decreased.

The photocatalytic network produced in this study provides a readily recoverable heterogeneous photocatalyst. However, the gel network produced in this study requires the diffusion of reagents into the network for degradation. To investigate the effect the diffusion has on the degradation rate of glyphosate, a linear polymer was synthesized. Here, the photocatalytic monomer was copolymerized with DMAA in the same ratio as in the hydrogel without usage of a cross-linker and was analyzed via H NMR and GPC (Figures S34 and S35). The photodegradation of glyphosate using the linear PDMAA shows a similar linear degradation with full conversion in under 120 min (Figures S36 and S37). The linear photocatalytic polymer had a slightly faster rate of degradation when

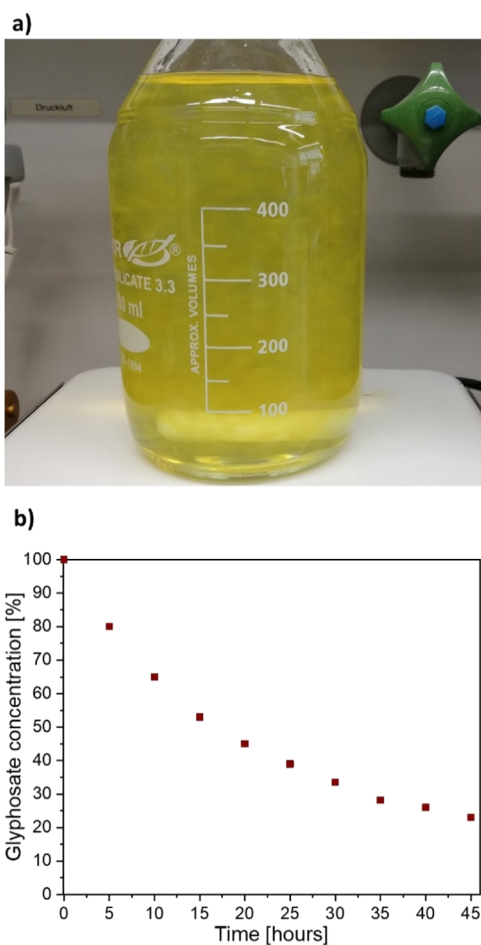


Figure 3. Large-scale glyphosate degradation. (a) 0.5 L scale photodegradation of 1 g of glyphosate in water. (b) glyphosate degradation over time monitored via ^{31}P NMR.

compared to the polymer gel network. However, the photocatalytic polymer hydrogel is much easier to recover making it a more favorable material for long-term use.

CONCLUSIONS

In summary, we present the radical copolymerization of a photocatalytic monomer into a highly transparent cross-linked hydrogel. This nontoxic water-compatible photocatalytic hydrogel has easily accessible photoactive centers within a high transmittance network. The transmittance of visible light to the active sites enables homogeneous photocatalysis over the whole material, as the polymer network does not interfere. This classical polymer photocatalyst was used for efficient water remediation of common pollutants in wastewater. We showcased the photoreduction Cr^{VI} and the photodegradation of glyphosate under visible light irradiation. Furthermore, high transmission hydrogels could be used on large scales, with glyphosate degradation conducted on the half liter scale. The combination of classic polymers with small molecule photocatalysts enables the production of tunable functional materials that can be used for a range of applications including wastewater remediation. The reported material could be used for the remediation of various wastewater compounds, while allowing for easy recycling of the bulky material. The created hydrogel allows for the fast uptake of wastewater pollutants and the rapid remediation. The bulky material further only

possesses a small amount of the photocatalytically active material, allowing for easy handling and scale up.

ASSOCIATED CONTENT

Supporting Information

The Supporting Information is available free of charge at <https://pubs.acs.org/doi/10.1021/acs.chemmater.1c02180>.

Further experimental measurements and characterization via NMR/ssNMR, FTIR, and cyclic voltammetry, photocurrent, DFT calculation, UV/Vis absorption, scavenger test, and GCMS (PDF)

AUTHOR INFORMATION

Corresponding Authors

Kai A. I. Zhang – Department of Materials Science, Fudan University, Shanghai 200433, P. R. China; orcid.org/0000-0003-0816-5718; Email: kai_zhang@fudan.edu.cn

Calum T. J. Ferguson – Max Planck Institute for Polymer Research, 55128 Mainz, Germany; orcid.org/0000-0002-6168-4624; Email: ferguson@mpip-mainz.mpg.de

Authors

Thomas Kuckhoff – Max Planck Institute for Polymer Research, 55128 Mainz, Germany

Katharina Landfester – Max Planck Institute for Polymer Research, 55128 Mainz, Germany; orcid.org/0000-0001-9591-4638

Complete contact information is available at: <https://pubs.acs.org/doi/10.1021/acs.chemmater.1c02180>

Funding

Open access funded by Max Planck Society.

Notes

The authors declare no competing financial interest.

ACKNOWLEDGMENTS

The Deutsche Forschungsgemeinschaft (DFG) is acknowledged for funding (ZH 478/5-1). The authors would also like to thank Niklas Huber for undertaking ssNMR measurements and Marina Melchior for undertaking microscopy.

REFERENCES

- (1) Rahman, M. Z.; Kibria, M. G.; Mullins, C. B. Metal-free photocatalysts for hydrogen evolution. *Chem. Soc. Rev.* **2020**, *49*, 1887–1931.
- (2) Rahman, M. Z.; Davey, K.; Qiao, S.-Z. Carbon, nitrogen and phosphorus containing metal-free photocatalysts for hydrogen production: progress and challenges. *J. Mater. Chem. A* **2018**, *6*, 1305–1322.
- (3) Bi, S.; Lan, Z.-A.; Paasch, S.; Zhang, W.; He, Y.; Zhang, C.; Liu, F.; Wu, D.; Zhuang, X.; Brunner, E.; Wang, X.; Zhang, F. Substantial Cyano-Substituted Fully sp²-Carbon-Linked Framework: Metal-Free Approach and Visible-Light-Driven Hydrogen Evolution. *Adv. Funct. Mater.* **2017**, *27*, 1703146.
- (4) Chen, W.; Wang, L.; Mo, D.; He, F.; Wen, Z.; Wu, X.; Xu, H.; Chen, L. Modulating Benzothiadiazole-Based Covalent Organic Frameworks via Halogenation for Enhanced Photocatalytic Water Splitting. *Angew. Chem., Int. Ed.* **2020**, *59*, 16902–16909.
- (5) Wang, Z.; Li, C.; Domen, K. Recent developments in heterogeneous photocatalysts for solar-driven overall water splitting. *Chem. Soc. Rev.* **2019**, *48*, 2109–2125.
- (6) Wang, X.; Maeda, K.; Thomas, A.; Takanabe, K.; Xin, G.; Carlsson, J. M.; Domen, K.; Antonietti, M. A metal-free polymeric

photocatalyst for hydrogen production from water under visible light. *Nat. Mater.* **2009**, *8*, 76–80.

(7) Liu, J.; Liu, Y.; Liu, N.; Han, Y.; Zhang, X.; Huang, H.; Lifshitz, Y.; Lee, S.-T.; Zhong, J.; Kang, Z. Metal-free efficient photocatalyst for stable visible water splitting via a two-electron pathway. *Science* **2015**, *347*, 970–974.

(8) Savateev, A.; Antonietti, M. Heterogeneous Organocatalysis for Photoredox Chemistry. *ACS Catal.* **2018**, *8*, 9790–9808.

(9) Li, R.; Ma, B. C.; Huang, W.; Wang, L.; Wang, D.; Lu, H.; Landfester, K.; Zhang, K. A. I. Photocatalytic Regioselective and Stereoselective [2 + 2] Cycloaddition of Styrene Derivatives Using a Heterogeneous Organic Photocatalyst. *ACS Catal.* **2017**, *7*, 3097–3101.

(10) Su, C.; Tandiana, R.; Tian, B.; Sengupta, A.; Tang, W.; Su, J.; Loh, K. P. Visible-Light Photocatalysis of Aerobic Oxidation Reactions Using Carbazolic Conjugated Microporous Polymers. *ACS Catal.* **2016**, *6*, 3594–3599.

(11) Li, R.; Byun, J.; Huang, W.; Ayed, C.; Wang, L.; Zhang, K. A. I. Poly(benzothiadiazoles) and Their Derivatives as Heterogeneous Photocatalysts for Visible-Light-Driven Chemical Transformations. *ACS Catal.* **2018**, *8*, 4735–4750.

(12) Su, F.; Mathew, S. C.; Möhlmann, L.; Antonietti, M.; Wang, X.; Blechert, S. Aerobic oxidative coupling of amines by carbon nitride photocatalysis with visible light. *Angew. Chem., Int. Ed.* **2011**, *50*, 657–660.

(13) Huang, W.; Byun, J.; Rörich, I.; Ramanan, C.; Blom, P. W. M.; Lu, H.; Wang, D.; Caire da Silva, L.; Li, R.; Wang, L.; Landfester, K.; Zhang, K. A. I. Asymmetric Covalent Triazine Framework for Enhanced Visible-Light Photoredox Catalysis via Energy Transfer Cascade. *Angew. Chem., Int. Ed.* **2018**, *57*, 8316–8320.

(14) Zhao, G.; Huang, X.; Wang, X.; Wang, X. Progress in catalyst exploration for heterogeneous CO₂ reduction and utilization: a critical review. *J. Mater. Chem. A* **2017**, *5*, 21625–21649.

(15) Cao, S.; Low, J.; Yu, J.; Jaroniec, M. Polymeric photocatalysts based on graphitic carbon nitride. *Adv. Mater.* **2015**, *27*, 2150–2176.

(16) Habisreutinger, S. N.; Schmidt-Mende, L.; Stolarczyk, J. K. Photocatalytic Reduction of CO₂ on TiO₂ and Other Semiconductors. *Angew. Chem., Int. Ed.* **2013**, *52*, 7372–7408.

(17) Fu, Y.; Zhu, X.; Huang, L.; Zhang, X.; Zhang, F.; Zhu, W. Azine-based covalent organic frameworks as metal-free visible light photocatalysts for CO₂ reduction with H₂O. *Appl. Catal., B* **2018**, *239*, 46–51.

(18) Konan, Y. N.; Gurny, R.; Allémann, E. State of the art in the delivery of photosensitizers for photodynamic therapy. *J. Photochem. Photobiol., B* **2002**, *66*, 89–106.

(19) Zhu, C.; Liu, L.; Yang, Q.; Lv, F.; Wang, S. Water-soluble conjugated polymers for imaging, diagnosis, and therapy. *Chem. Rev.* **2012**, *112*, 4687–4735.

(20) He, C.; Duan, X.; Guo, N.; Chan, C.; Poon, C.; Weichselbaum, R. R.; Lin, W. Core-shell nanoscale coordination polymers combine chemotherapy and photodynamic therapy to potentiate checkpoint blockade cancer immunotherapy. *Nat. Commun.* **2016**, *7*, 12499.

(21) Lucky, S. S.; Soo, K. C.; Zhang, Y. Nanoparticles in photodynamic therapy. *Chem. Rev.* **2015**, *115*, 1990–2042.

(22) Ahmed, S. N.; Haider, W. Heterogeneous photocatalysis and its potential applications in water and wastewater treatment: a review. *Nanotechnology* **2018**, *29*, 342001.

(23) Byun, J.; Landfester, K.; Zhang, K. A. I. Conjugated Polymer Hydrogel Photocatalysts with Expandable Photoactive Sites in Water. *Chem. Mater.* **2019**, *31*, 3381–3387.

(24) Marin, M. L.; Santos-Juanes, L.; Arques, A.; Amat, A. M.; Miranda, M. A. Organic photocatalysts for the oxidation of pollutants and model compounds. *Chem. Rev.* **2012**, *112*, 1710–1750.

(25) Ahmed, S.; Rasul, M. G.; Martens, W. N.; Brown, R.; Hashib, M. A. Heterogeneous photocatalytic degradation of phenols in wastewater: A review on current status and developments. *Desalination* **2010**, *261*, 3–18.

(26) Zheng, Q.; Durkin, D. P.; Elenewski, J. E.; Sun, Y.; Banek, N. A.; Hua, L.; Chen, H.; Wagner, M. J.; Zhang, W.; Shuai, D. Visible-

Light-Responsive Graphitic Carbon Nitride: Rational Design and Photocatalytic Applications for Water Treatment. *Environ. Sci. Technol.* **2016**, *50*, 12938–12948.

(27) Andreozzi, R.; Raffaele, M.; Nicklas, P. Pharmaceuticals in STP effluents and their solar photodegradation in aquatic environment. *Chemosphere* **2003**, *50*, 1319–1330.

(28) Petrie, B.; Barden, R.; Kasprzyk-Hordern, B. A review on emerging contaminants in wastewaters and the environment: current knowledge, understudied areas and recommendations for future monitoring. *Water Res.* **2015**, *72*, 3–27.

(29) Shen, J.; Steinbach, R.; Tobin, J. M.; Mouro Nakata, M.; Bower, M.; McCoustra, M. R. S.; Bridle, H.; Arrighi, V.; Vilela, F. Photoactive and metal-free polyamide-based polymers for water and wastewater treatment under visible light irradiation. *Appl. Catal., B* **2016**, *193*, 226–233.

(30) Chen, S.; Liu, Y. Study on the photocatalytic degradation of glyphosate by TiO₂ photocatalyst. *Chemosphere* **2007**, *67*, 1010–1017.

(31) Koe, W. S.; Lee, J. W.; Chong, W. C.; Pang, Y. L.; Sim, L. C. An overview of photocatalytic degradation: photocatalysts, mechanisms, and development of photocatalytic membrane. *Environ. Sci. Pollut. Res. Int.* **2020**, *27*, 2522–2565.

(32) Ghosh, S.; Kouamé, N. A.; Ramos, L.; Remita, S.; Dazzi, A.; Deniset-Besseau, A.; Beaunier, P.; Goubard, F.; Aubert, P.-H.; Remita, H. Conducting polymer nanostructures for photocatalysis under visible light. *Nat. Mater.* **2015**, *14*, 505–511.

(33) He, X.; Wu, Z.; Xue, Y.; Gao, Z.; Yang, X. Fabrication of interlayer β -CD/g-C₃N₄@MoS₂ for highly enhanced photodegradation of glyphosate under simulated sunlight irradiation. *RSC Adv.* **2019**, *9*, 4635–4643.

(34) Manassero, A.; Satuf, M. L.; Alfano, O. M. Photocatalytic reactors with suspended and immobilized TiO₂: Comparative efficiency evaluation. *Chem. Eng. J.* **2017**, *326*, 29–36.

(35) Yang, C.; Li, R.; Zhang, K. A. I.; Lin, W.; Landfester, K.; Wang, X. Heterogeneous photoredox flow chemistry for the scalable organosynthesis of fine chemicals. *Nat. Commun.* **2020**, *11*, 1239.

(36) Sivagami, K.; Vikraman, B.; Krishna, R. R.; Swaminathan, T. Chlorpyrifos and Endosulfan degradation studies in an annular slurry photo reactor. *Ecotoxicol. Environ. Saf.* **2016**, *134*, 327–331.

(37) Berberidou, C.; Kitsiou, V.; Kazala, E.; Lambropoulou, D. A.; Kouras, A.; Kosma, C. I.; Albanis, T. A.; Poullos, I. Study of the decomposition and detoxification of the herbicide bentazon by heterogeneous photocatalysis: Kinetics, intermediates and transformation pathways. *Appl. Catal., B* **2017**, *200*, 150–163.

(38) Yun, J.; Im, J. S.; Oh, A.; Jin, D.-H.; Bae, T.-S.; Lee, Y.-S.; Kim, H.-I. pH-sensitive photocatalytic activities of TiO₂/poly(vinyl alcohol)/poly(acrylic acid) composite hydrogels. *Mater. Sci. Eng., B* **2011**, *176*, 276–281.

(39) Yang, J.; Gao, J.; Wang, X.; Mei, S.; Zhao, R.; Hao, C.; Wu, Y.; Zhai, X.; Liu, Y. Polyacrylamide hydrogel as a template in situ synthesis of CdS nanoparticles with high photocatalytic activity and photostability. *J. Nanopart. Res.* **2017**, *19*, 350.

(40) Ghasimi, S.; Prescher, S.; Wang, Z. J.; Landfester, K.; Yuan, J.; Zhang, K. A. I. Heterophase Photocatalysts from Water-Soluble Conjugated Polyelectrolytes: An Example of Self-Initiation under Visible Light. *Angew. Chem., Int. Ed.* **2015**, *54*, 14549–14553.

(41) Liu, Z.; Su, Q.; Ju, P.; Li, X.; Li, G.; Wu, Q.; Yang, B. A hydrophilic covalent organic framework for photocatalytic oxidation of benzylamine in water. *Chem. Commun.* **2020**, *56*, 766–769.

(42) Wang, X.; Liang, Y.; An, W.; Hu, J.; Zhu, Y.; Cui, W. Removal of chromium (VI) by a self-regenerating and metal free g-C₃N₄/graphene hydrogel system via the synergy of adsorption and photocatalysis under visible light. *Appl. Catal., B* **2017**, *219*, 53–62.

(43) Nuhn, L.; Hirsch, M.; Krieg, B.; Koynov, K.; Fischer, K.; Schmidt, M.; Helm, M.; Zentel, R. Cationic Nanohydrogel Particles as Potential siRNA Carriers for Cellular Delivery. *ACS Nano* **2012**, *6*, 2198–2214.

- (44) Kopecek, J. Hydrogels: From soft contact lenses and implants to self-assembled nanomaterials. *J. Polym. Sci., Part A: Polym. Chem.* **2009**, *47*, 5929–5946.
- (45) Burdick, J. A.; Murphy, W. L. Moving from static to dynamic complexity in hydrogel design. *Nat. Commun.* **2012**, *3*, 1269.
- (46) Peng, C.-C.; Kim, J.; Chauhan, A. Extended delivery of hydrophilic drugs from silicone-hydrogel contact lenses containing vitamin E diffusion barriers. *Biomaterials* **2010**, *31*, 4032–4047.
- (47) Xinming, L.; Yingde, C.; Lloyd, A. W.; Mikhailovsky, S. V.; Sandeman, S. R.; Howel, C. A.; Liewen, L. Polymeric hydrogels for novel contact lens-based ophthalmic drug delivery systems: a review. *Contact Lens Anterior Eye* **2008**, *31*, 57–64.
- (48) Qi, X.; Wei, W.; Su, T.; Zhang, J.; Dong, W. Fabrication of a new polysaccharide-based adsorbent for water purification. *Carbohydr. Polym.* **2018**, *195*, 368–377.
- (49) Bekiari, V.; Lianos, P. Ureasil Gels as a Highly Efficient Adsorbent for Water Purification. *Chem. Mater.* **2006**, *18*, 4142–4146.
- (50) Ferguson, C. T. J.; Huber, N.; Landfester, K.; Zhang, K. A. I. Dual-Responsive Photocatalytic Polymer Nanogels. *Angew. Chem.* **2019**, *131*, 10677.
- (51) Huber, N.; Li, R.; Ferguson, C. T. J.; Gehrig, D. W.; Ramanan, C.; Blom, P. W. M.; Landfester, K.; Zhang, K. A. I. A PMMA-based heterogeneous photocatalyst for visible light-promoted [4 + 2] cycloaddition. *Catal. Sci. Technol.* **2020**, *10*, 2092–2099.
- (52) Ferguson, C. T. J.; Huber, N.; Kuckhoff, T.; Zhang, K. A. I.; Landfester, K. Dispersible porous classical polymer photocatalysts for visible light-mediated production of pharmaceutically relevant compounds in multiple solvents. *J. Mater. Chem. A* **2020**, *8*, 1072–1076.
- (53) Ferguson, C. T. J.; Zhang, K. A. I. Classical Polymers as Highly Tunable and Designable Heterogeneous Photocatalysts. *ACS Catal.* **2021**, *11*, 9547–9560.
- (54) Zhao, W.; Yang, C.; Huang, J.; Jin, X.; Deng, Y.; Wang, L.; Su, F.; Xie, H.; Wong, P. K.; Ye, L. Selective aerobic oxidation of sulfides to sulfoxides in water under blue light irradiation over Bi₄O₅Br₂. *Green Chem.* **2020**, *22*, 4884–4889.
- (55) Akpor, O. B.; Ohiobor, G. O.; Olaolu, T. D. Heavy Metal Pollutants in Wastewater Effluents: Sources, Effects and Remediation. *Adv. Biosci. Bioeng.* **2014**, *2*, 37–43.
- (56) Barakat, M. A. New trends in removing heavy metals from industrial wastewater. *Arabian J. Chem.* **2011**, *4*, 361–377.
- (57) Kieber, R. J.; Willey, J. D.; Zvalaren, S. D. Chromium Speciation in Rainwater: Temporal Variability and Atmospheric Deposition. *Environ. Sci. Technol.* **2002**, *36*, 5321–5327.
- (58) Shanker, A.; Cervantes, C.; Lozavera, H.; Avudainayagam, S. Chromium toxicity in plants. *Environ. Int.* **2005**, *31*, 739–753.
- (59) Zhitkovich, A. Chromium in drinking water: sources, metabolism, and cancer risks. *Chem. Res. Toxicol.* **2011**, *24*, 1617–1629.
- (60) Ghasimi, S.; Landfester, K.; Zhang, K. A. I. Water Compatible Conjugated Microporous Polyazulene Networks as Visible-Light Photocatalysts in Aqueous Medium. *ChemCatChem* **2016**, *8*, 694–698.
- (61) Chen, W.; Yang, Z.; Xie, Z.; Li, Y.; Yu, X.; Lu, F.; Chen, L. Benzothiadiazole functionalized D-A type covalent organic frameworks for effective photocatalytic reduction of aqueous chromium(vi). *J. Mater. Chem. A* **2019**, *7*, 998–1004.
- (62) Woodburn, A. T. Glyphosate: production, pricing and use worldwide. *Pest Manage. Sci.* **2000**, *56*, 309–312.
- (63) Baylis, A. D. Why glyphosate is a global herbicide: strengths, weaknesses and prospects. *Pest Manage. Sci.* **2000**, *56*, 299–308.
- (64) Hébert, M.-P.; Fugère, V.; Gonzalez, A. The overlooked impact of rising glyphosate use on phosphorus loading in agricultural watersheds. *Front. Ecol. Environ.* **2019**, *17*, 48–56.
- (65) Battaglin, W. A.; Kolpin, D. W.; Scribner, E. A.; Kuivila, K. M.; Sandstrom, M. W. Glyphosate, Other Herbicides, and Transformation Products in Midwestern Streams, 20021. *J. Am. Water Resour. Assoc.* **2005**, *41*, 323–332.
- (66) Poiger, T.; Buerge, I. J.; Bächli, A.; Müller, M. D.; Balmer, M. E. Occurrence of the herbicide glyphosate and its metabolite AMPA in surface waters in Switzerland determined with on-line solid phase extraction LC-MS/MS. *Environ. Sci. Pollut. Res. Int.* **2017**, *24*, 1588–1596.
- (67) Toss, V.; Leito, I.; Yurchenko, S.; Freiberg, R.; Kruve, A. Determination of glyphosate in surface water with high organic matter content. *Environ. Sci. Pollut. Res. Int.* **2017**, *24*, 7880–7888.
- (68) Tsui, M. T. K.; Chu, L. M. Aquatic toxicity of glyphosate-based formulations: comparison between different organisms and the effects of environmental factors. *Chemosphere* **2003**, *52*, 1189–1197.
- (69) Annett, R.; Habibi, H. R.; Hontela, A. Impact of glyphosate and glyphosate-based herbicides on the freshwater environment. *J. Appl. Toxicol.* **2014**, *34*, 458–479.
- (70) Lund-Høie, K.; Friestad, H. O. Photodegradation of the Herbicide Glyphosate in Water. *Bull. Environ. Contam. Toxicol.* **1986**, *36*, 723–729.
- (71) Huo, R.; Yang, X.-L.; Yang, J.-Y.; Yang, S.-Y.; Xu, Y.-H. Self-assembly synthesis of BiVO₄/Polydopamine/g-C₃N₄ with enhanced visible light photocatalytic performance. *Mater. Res. Bull.* **2018**, *98*, 225–230.
- (72) Kudzin, M.; Żyła, R.; Mrozińska, Z.; Urbaniak, P. 31P NMR Investigations on Roundup Degradation by AOP Procedures. *Water* **2019**, *11*, 331.